Future Expansion of the Pacific Oxygen Minimum Zone

Julius J.M. Busecke[1], **Laure Resplandy**[2]**and Jasmin G. John**[3]

[1]Columbia University
[2]Princeton University
[3]NOAA/OAR/Geophysical Fluid Dynamics Laboratory

Key Points:

- The Pacific Oxygen Minimum Zone (OMZ) will expand in response to anthropogenic forcing.
- Expansion is controlled by reduction of shallow overturning circulation and oxygen supply to the upper OMZ.
- Uncertainties in expansion magnitude draw from both physical and biological processes in the lower OMZ.

Corresponding author: Julius Busecke, julius@ldeo.columbia.edu

Abstract

Global ocean oxygen loss - deoxygenation - is projected to persist in the future. Previous generations of Earth system models (ESMs) have, however, failed to provide a consistent picture of how deoxygenation will influence oxygen minimum zones (OMZs; $O_2 <= 80\,\mu mol/kg$), in particular the largest OMZ in the tropical Pacific Ocean. The expansion of the Pacific OMZ would threaten marine ecosystems and ecosystem services such as fisheries and could amplify climate change by emitting greenhouse gases. Here, we use the latest generation of ESMs (CMIP6) and a density framework that isolates oxygen changes in the thermocline and intermediate waters. We show that the Pacific OMZ expands by the end of the century in response to high anthropogenic emissions (multi-ESM median expansion of $2.4^{15}\,m^3$, about 4% of the observed OMZ volume). The expansion is driven by a reduction of the shallow overturning circulation in the thermocline and a robust weakening of the oxygen supply to the upper OMZ in all ESMs. The magnitude of this expansion is, however, uncertain due to the less constrained balance between physical and biological changes in the lower OMZ. Despite uncertainties in the biological response, our results suggest that models with more complex biogeochemistry project weaker changes in the lower OMZ, and therefore stronger overall OMZ expansion. The fact that the OMZ largely expands in the upper ocean maximizes its ecological, economic, and climatic impacts (release of greenhouse gases).

Plain Language Summary

Expansion of ocean areas with low oxygen concentrations threatens marine animals and can also increase the production of greenhouse gases that warm the Earth. An essential question is how these low oxygen "blobs", called oxygen minimum zones, will evolve in the future. Oxygen minimum zones are difficult to simulate in climate models because they result from two strongly opposing processes: Physical supply of oxygen via the ocean circulation and oxygen consumption by decomposing biology. Previous studies using older generations of models could not conclude whether the largest of these zones in the Pacific would grow or shrink in the future. We show that the Pacific oxygen minimum zone will grow in response to climate change: all models agree that the upper part of this low oxygen 'blob' will grow, while the lower part will either not change or contract slightly. This is potentially bad news for the marine species that suffer in low oxygen conditions, the people that depend on them (fishing, tourism), and the global climate.

1 Introduction

The ocean has lost dissolved oxygen (O_2) in response to global warming in the past 50 years (∼2% globally; Keeling et al. (2010); Ito et al. (2017); Schmidtko et al. (2017); Levin (2018)). A serious threat of this systematic ocean deoxygenation is the expansion of tropical oxygen minimum zones (OMZs), where low O_2 levels threaten marine life (Vaquer-Sunyer & Duarte, 2008; Stramma et al., 2012; do Rosário Gomes et al., 2014) and perturb the carbon and nitrogen cycles, potentially acting as an amplifying feedback on climate change (Stramma et al., 2008; Keeling et al., 2010; Levin, 2018). Global upper ocean deoxygenation is projected to continue in the 21st century, especially if greenhouse gas emissions are not rapidly curtailed (Bopp et al., 2013; Kwiatkowski et al., 2020). There is, however, no consensus on how the OMZs will evolve in the future (e.g., Resplandy (2018)).

The Tropical Pacific Ocean hosts the largest OMZ in the global ocean. Its expansion would certainly threaten the habitat and survival of marine life, including species vital to local and global marine ecosystem services (e.g., anchovies and sardines, (Bertrand et al., 2011; Chavez et al., 2008)). A larger OMZ would also increase the production of nitrous oxide; a powerful greenhouse gas (Babbin et al., 2015; Yang et al., 2017) And in-

crease the removal of biologically available nitrogen (Lam & Kuypers, 2011), which in turn could limit the efficiency of the ocean's biological carbon sink.

Uncertainties in the spatial and temporal evolution of the Pacific OMZ severely restrict our ability to anticipate its ecological, climatic, and societal impacts. Observations suggest that the Pacific OMZ shrunk for most of the 20th century but expanded after 1970 (Stramma et al., 2008; Deutsch et al., 2014). Earth system models (ESMs) from the Climate Model Intercomparison Project phase 5 (CMIP5; Taylor et al. (2011)) projected contradicting trends, in which the Pacific OMZ could either expand or shrink with volume changes between -15% and +15% (Cabré et al., 2015).

These ESMs projected an O_2 loss in response to ocean warming, which makes O_2 less soluble in surface waters and limits their transfer to the deeper ocean and the ventilation of the ocean interior (Cabré et al., 2015; Bopp et al., 2017; Kwiatkowski et al., 2020). They also consistently projected reduction in the O_2 demand in the subsurface, tied to weaker biological productivity and particle export to depth (Bopp et al., 2013; Kwiatkowski et al., 2020). Yet, this generation of ESMs disagreed on how strongly changes in ocean ventilation and biological activity offset each other in space and time, leading to either the contraction or the expansion of the OMZ (Cabré et al., 2015; Frölicher et al., 2020). The influence of ocean circulation emerged as a particularly important factor in these uncertainties. For instance, ESMs that projected a larger expansion of the OMZ in the equatorial Pacific by the year 2100 were those that simulated a stronger decline in the equatorial Pacific circulation, largely exceeding the biological changes (Shigemitsu et al., 2017).

The Pacific OMZ is found in the so-called 'shadow zones' of the subsurface ocean (∼200-2000 m, Figure 1), characterized by weak ventilation, long water residence time (Luyten et al., 1983; Pedlosky, 1986) and highly productive surface upwelling systems that boost O_2 biological demand at the subsurface (Paulmier & Ruiz-Pino, 2009). It extends over two distinct dynamical regimes governed by different processes and on different timescales. The upper part of the OMZ is located in the thermocline (within the upper 600m-1000m) and is influenced by the advective flow associated with the shallow overturning and the zonal currents near the Equator (Duteil et al., 2014; J. J. M. Busecke et al., 2019). The majority of the OMZ volume resides at intermediate depth (up to 2000m depth) where the overturning circulation is less energetic and where slow mixing (isopycnal and diapycnal) plays a crucial role in supplying O_2 and balancing the consumption by respiration (Duteil & Oschlies, 2011; Bahl et al., 2019; Lévy et al., 2021).

The fact that the OMZ extends over these two distinct regimes makes it particularly challenging to isolate and interpret OMZ projections and contributes to the uncertainties in the OMZ evolution. In this study, we investigate forced changes in the Pacific Ocean OMZ volume using the latest generation of ESMs (CMIP6, Eyring et al. (2016)) and a density framework that distinguishes between changes in the OMZ within the thermocline and the intermediate waters. We show that ESMs project a consistent expansion of the Pacific OMZ by 2100, dominated by the growth of the OMZ in the thermocline, while changes in the intermediate waters play only a secondary role by modulating the magnitude of the expansion.

2 Methods

2.1 CMIP6 Earth System Models and Observations

We used the 14 ESMs from the CMIP6 archive that made monthly outputs of ocean oxygen, potential temperature, salinity, and meridional velocity available for the preindustrial control, the historical period, and the high-emission scenario SSP5-8.5 via the Earth System Grid Federation (ESGF; Petrie et al. (2021)) (see Table 1 for models and variables used). Our results consider the period from 1850-2100. We used additional vari-

ables that were not available for all of the models: Mixed layer depth (mlotst; available for 12 ESMs), particulate carbon export at 100m (epc100; available for 13 ESMs), ideal water age (variable *agessc*; available for 13 ESMs). For details on availability see Table 1.

We additionally disregarded the ideal age from 3 ESMs (MPI-ESM1-2-HR, MRI-ESM2-0, UKESM1-0-LL) and some members of MPI-ESM1-2-LR in which *agessc* was re-initialized to zero at the beginning of the historical and/or the SSP5-8.5 simulations as these could not be used to evaluate the changes in watermass age. We developed and used the 'cmip6_preprocessing' python package (J. Busecke & Spring, 2020) to preprocess the CMIP6 ESM data (e.g., homogenize naming, units, metadata/reconstruct missing grid metrics/masking ocean basins) in conjunction with a custom 'intake-esm' (Banihirwe et al., 2020) catalog which enables easy management of the large amount of data used in this study (100+ TB). To reduce the effects of model drift, all variables were detrended using the linear trend of the preindustrial control run at every grid point for each ESM member. When variables were not provided on the native ocean model grid (indicated by 'gr' in Table 1), we linearly interpolate values onto the native grid using the 'xESMF' python package (Zhuang et al., 2021). Values within the mixed layer and in the bottom cells were not considered in this analysis to avoid issues with partial bottom cells and exclude values near topography from the analysis for all ESMs.

We used observations of potential temperature (Locarnini et al., 2013), salinity (Zweng, 2013) and O_2 (Garcia et al., 2013) from the World Ocean Atlas 2013.

2.2 Diagnosing OMZ thickness, volume, and natural variability

To diagnose the vertical thickness and volume of the OMZ, we converted O_2 values into $\mu mol/kg$ using a constant reference density of $\rho_0 = 1025\,kg/m^3$. We then computed the OMZ thickness H_{OMZ} at each point in space and the total OMZ volume V_{OMZ} in the tropical Pacific Ocean using the ESM grid cell thickness and horizontal area where O_2 concentrations <= 80 $\mu mol/kg$. If not otherwise mentioned, the analysis (average, median, integrals, etc.) is performed for the Tropical Pacific ($30°S$-$30°N$). We quantified the OMZ volume natural variability from interannual to multi-decadal timescales in each ESM based on the last 300 years of the preindustrial control run. For each ESM member, we estimate the natural variability as ± 2 standard deviation in time of the linearly detrended OMZ volume. For ESMs with multiple control run members, we average the standard deviations over all available members. The upper bound of natural variability is defined as the largest natural value across all ESM control runs.

2.3 Density framework

Our analysis considers three density layers defined using the potential density anomaly with respect to the surface (σ_0):

- The 'thermocline' ($\sigma_0 = 24.5{-}26.5\,kg/m^3$). This layer includes subtropical mode waters in the pacific (Talley et al., 2011). In the observations this layer extends from $110 \pm 45\,m$ to $340 \pm 100\,m$ within the investigated domain.
- The 'intermediate waters' ($\sigma_0 = 26.5{-}27.65\,kg/m^3$), which includes subantarctic mode waters and intermediate waters (Talley et al., 2011). In the observations this layer extends from $340 \pm 100\,m$ to $1890 \pm 40\,m$ within the investigated domain.
- The 'deep ocean' ($\sigma_0 > 27.65\,kg/m^3$) In the observations this layer extends from $1890 \pm 40\,m$ to the ocean floor.

This isopycnal framework minimizes the effects of temperature change on oxygen concentrations (temperature is largely conserved along isopycnals in the tropical ocean) (Long et al., 2016).

We computed the σ_0 from potential temperature, and ocean salinity using the 'fastjmd95' python package (R. Abernathey, 2021). The transformation of variables into density space uses the 'xgcm' python package (R. Abernathey et al., 2020) We note that the total OMZ volume is conserved when transforming into density coordinates.

2.4 Distinguishing between physical and biological drivers of O_2 changes

We evaluated if changes in O_2 can be attributed to changes in physical or biological processes. We used changes in the ideal age tracer *agessc* available for 10 ESMs (see Table 1) as an indicator of circulation and ventilation changes and changes in oxygen utilization rate (OUR) as an indicator of biological changes. OUR is a proxy for the integrated oxygen utilization along a water parcel pathway since it was last in contact with the atmosphere ($\Delta OUR < 0$ indicates less O_2 demand). $OUR = AOU/age$ was computed using the apparent oxygen utilization $AOU = O_{2,sat} - O_2$, where $O_{2,sat}$ is the saturation oxygen concentration in seawater, calculated with the 'GSW-Python' package (Firing et al., 2021).

Changes in OUR, *agessc*, and AOU per century were computed as linear trends over the time period 2000-2100. For this study, we attributed the changes to either physical or biological processes if the sign of the O_2 change in one density layer was consistent with the sign of change of *agessc* (physical) or OUR (biological). If the change in O_2 was consistent with both *agessc* and OUR, we attributed it to both physical and biological changes. As discussed in the main text, this method is qualitative and subject to bias (e.g., OUR is not a perfect proxy of biological respiration). A more quantitative investigation of the physical and biological influences on the OMZ volume would require additional ESM diagnostics not available from the CMIP6 archive.

2.5 Subtropical overturning circulation and Subtrotropical Cell Index

To evaluate the large scale changes in the Pacific Ocean subtropical circulation we use the Subtropical Cell Index (STCI; Duteil et al. (2014)) which quantifies the mass transport from the subtropics into the equatorial area in both hemispheres as:

$$STCI = \Psi_{max} - \Psi_{min} \tag{1}$$

with Ψ_{max} and Ψ_{min} the maximum and minimum of the mass overturning streamfunction Ψ in the upper 250 meters and between 10°S and 10°N in the Pacific basin. Ψ at a latitude y and depth z is reconstructed as:

$$\Psi(y,z) = -\int_{z_0}^{z}\int_{x} vm(x,y,z')\,dx\,dz' \tag{2}$$

where z_0 is the ocean surface, and the vertically integrated meridional transport is approximated from the monthly meridional velocity v (linearly interpolated to a 1/4° by 1/4° for the pacific basin only) and the grid cell thickness h as $vm = v\,h$. To focus on large-scale patterns, we smoothed the Ψ with a ∼2 degrees latitudinal filter.

3 Results/Discussion

3.1 Representation of the historical Pacific OMZ

The OMZ ($O_2 < 80\mu mol/kg$) in observations is confined to the central and eastern Pacific and to the two density layers defined here as the thermocline ($\sigma_0 = 24.5-$

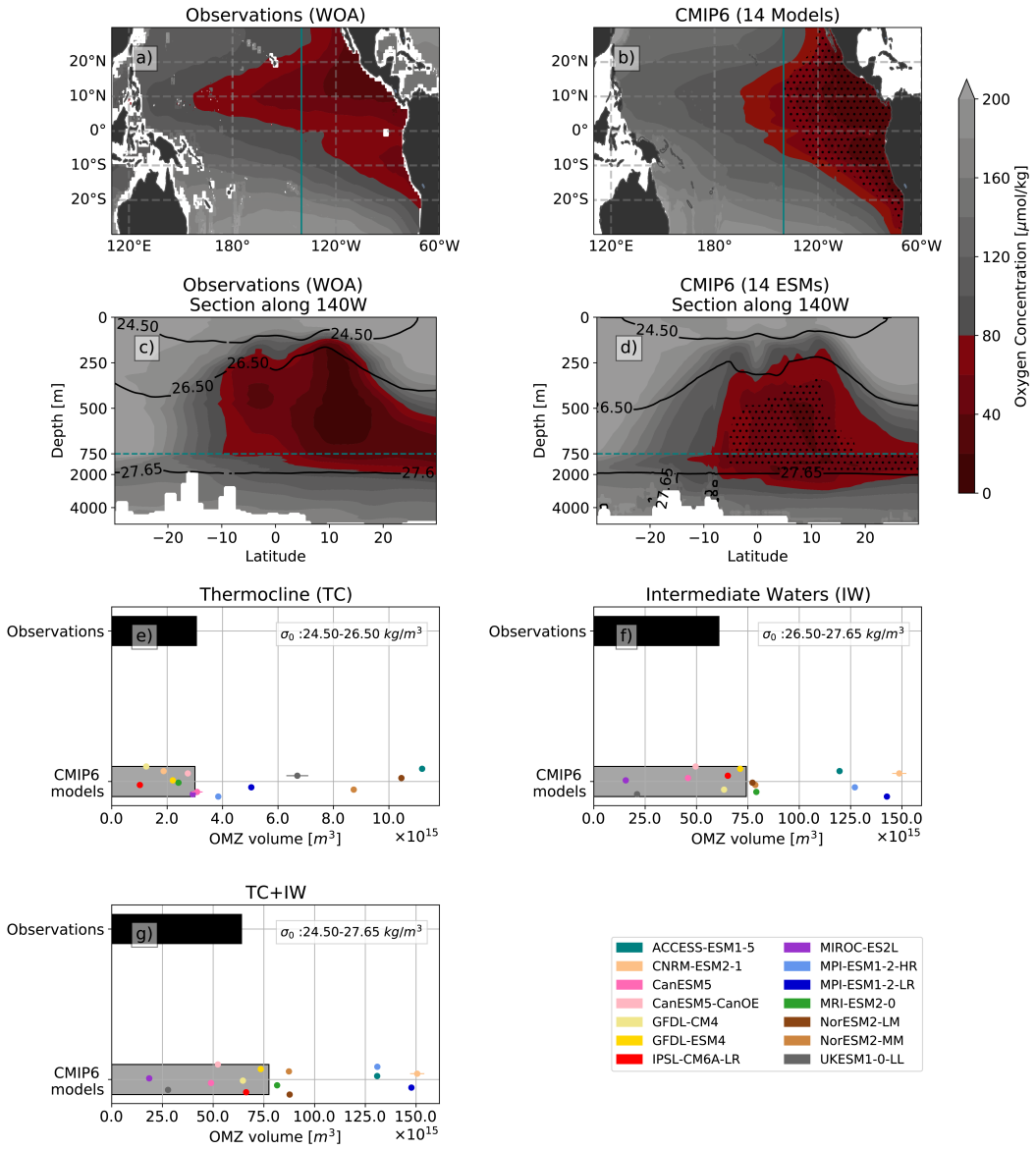

Figure 1: Historical OMZ in the tropical Pacific Ocean (1960-2000). O_2 distribution from observations (World Ocean Atlas 2013) and 14 CMIP6 ESMs: **a-b**) averaged over thermocline and intermediate waters (σ_0:24.5-27.65), **c-d**) along a depth section at 140°W (indicated by teal line in panels a,b). Panels a-d show OMZ (O_2 <= 80 μmol/kg in red), density (black contours), and areas where at least 11 of the 14 ESMs simulate an OMZ (stippling). **e-g**) OMZ volume in the thermocline (σ_0:24.5-26.5), intermediate waters (σ_0:26.5-27.65) and both combined for observations (black bar), individual ESMs (colored symbols) and ESM median (grey bar). Symbols are randomly shifted along the y axis to improve readability. Circles represent the mean of members where appropriate (±1 standard deviation across members is indicated as horizontal bars).

26.5 kg/m^3) and intermediate waters (σ_0 = 26.5 − 27.65kg/m^3), with about 95% of the OMZ volume in the intermediate waters ($61.2\times10^{15}m^3$ compared to $3.1\times10^{15}m^3$ in the thermocline, Figure 1). It shows a strong asymmetry between the northern hemisphere where O_2 concentrations are lower and the OMZ extends west of 180°E and the

southern hemisphere where it is confined east of ∼120°W (Figure 1 a). Along the equator, O_2 concentrations are higher than off of the equator (Figure 1a and c) due to the supply of oxygenated water by the equatorial current system (Stramma et al., 2010), particularly the Equatorial Undercurrent (J. J. M. Busecke et al., 2019).

All 14 ESMs in this study represent hypoxic waters in the tropical Pacific (Figure1 a-d). The multi-ESM median reproduces the observed OMZ volume in the thermocline ($3.0 \times 10^{15} m^3$; Figure 1e) and slightly overestimates the OMZ volume in the intermediate waters ($74.3 \times 10^{15} m^3$, i.e. ∼21% more than observed; Figure 1f). The shape and volume of the OMZ differ substantially between ESMs, with simulated volume (thermocline and intermediate waters combined) ranging from -71% to +134% of the observed volume (Figure 1g) and some ESMs capturing a more realistic spatial distribution of the OMZ than others (see Figure A1 and A2 for details on each ESM). The ESM ensemble captures some of the north-south asymmetry in the OMZ, with more than 75% of the ESMs representing an OMZ extending further west in the northern hemisphere than the southern hemisphere. The north-south asymmetry and the higher O_2 concentrations along the equator are, however, underestimated (Figure 1 b/d), likely due to shortcomings in the representation of the Equatorial current system and subtropical-tropical subduction pathways (Harper, 2000; Llanillo et al., 2018; J. J. M. Busecke et al., 2019).

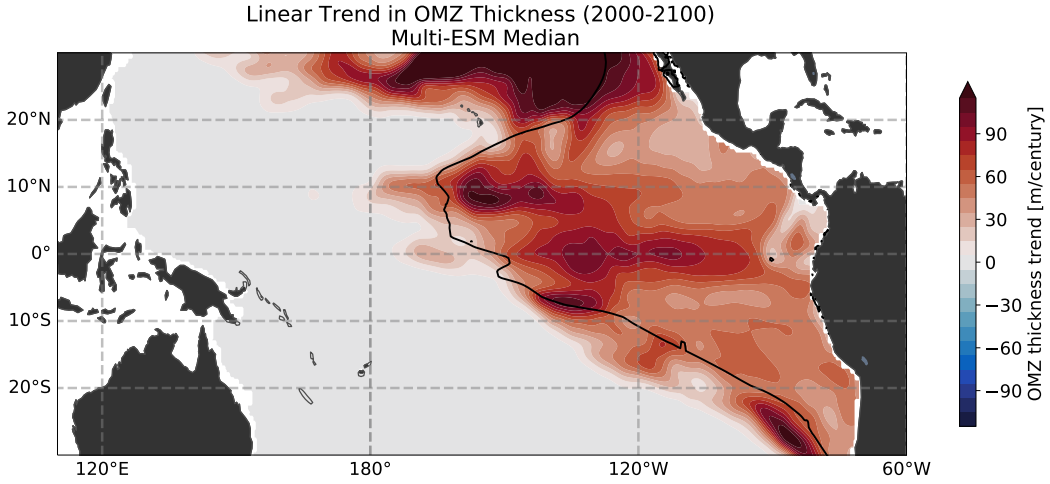

Figure 2: OMZ expansion for historical and SSP5-8.5 experiment. Changes in OMZ thickness (color, multi-ESM median smoothed with 1 degree gaussian kernel) and OMZ historical extent (80 μmol/kg contour, multi-ESM median).

3.2 Future OMZ expansion

One of the crucial questions is whether the Pacific OMZ will expand in the future. The ESM ensemble shows an increase in OMZ thickness of 10-100 m over most of the Eastern and Central Pacific by 2100 (Figure 2). This increase in thickness translates into a median increase in volume of $2.4 \pm 4.6 \times 10^{15} m^3$ (Figure 3d), equivalent to an expansion of the OMZ volume of about 4%, compared to the observed volume (Figure 1g). This expansion is primarily controlled by the consistent and well-constrained increase in volume in the thermocline ($3.3 \pm 0.9 \times 10^{15} m^3$), which outweighs the smaller contraction projected by the ESM ensemble in intermediate waters ($-1.2 \pm 4.2 \times 10^{15} m^3$; Figure 3e). The expansion in the thermocline exceeds the natural variability for all ESMs by the end of the century, and for most models, the signal emerges before 2020 (Figure 3a).

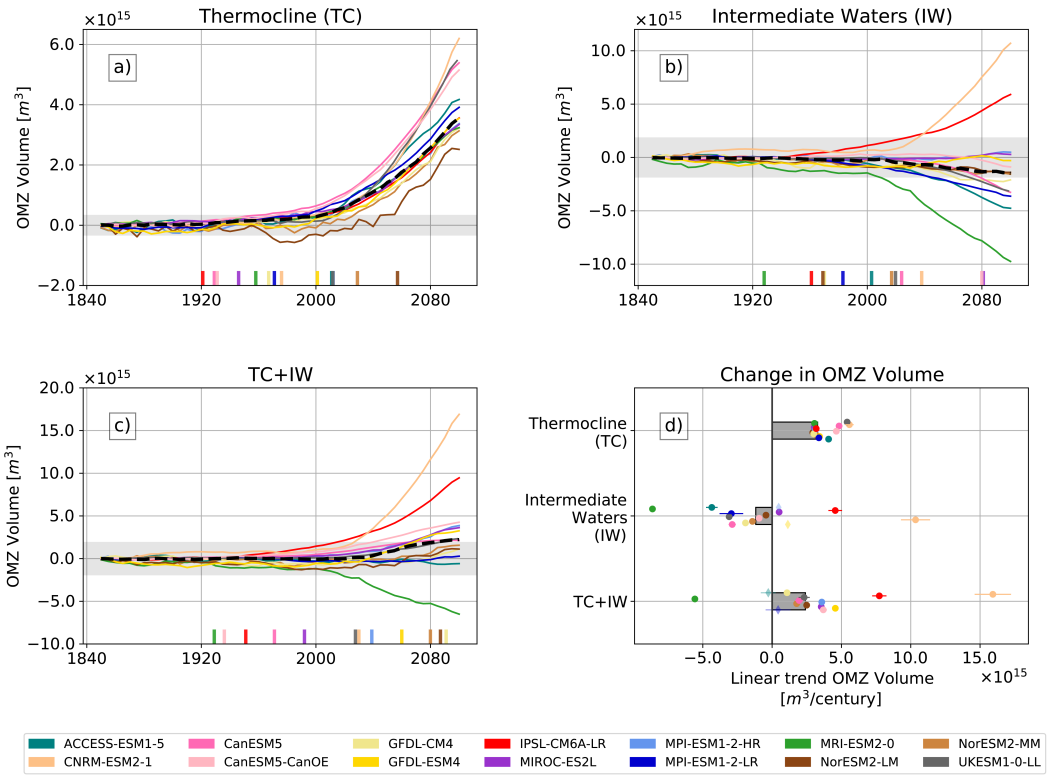

Figure 3: **a-c)** Evolution of OMZ volume for historical and SSP5-8.5 experiment in (a) thermocline, (b) intermediate waters, and (c) sum of both layers. Multi-ESM median (black dashed line) and upper bound of natural variability diagnosed from the ESM ensemble preindustrial control runs (shading) are indicated. Colored ticks indicate the time when the volume change exceeds the natural variability for each ESM. **d)** Change in OMZ volume projected for the multi-ESM median (grey bars) and the individual 14 ESMs (symbols). Symbols are randomly shifted along the y axis to improve readability. Where multiple members are available, symbols indicate member means, and error bars indicate ±1 standard deviation between members. Transparent diamonds indicate ESMs with trends that do not exceed natural variability.

The changes simulated in intermediate waters are more uncertain and modulate the magnitude of the overall expansion (Figure 3c, d). The majority of ESMs project a decrease in OMZ volume in intermediate waters smaller or equal to the expansion in the thermocline, resulting in an overall expansion for 11 ESMs and near-zero changes for 2 ESMs (changes smaller than natural variability, see diamond symbols in Figure3 d).

Four ESMs stand out within the intermediate waters: two simulate an OMZ contraction that matches or exceeds the expansion in the thermocline (MRI-ESM2-0 and ACCESS-ESM1-5; Figure 3d), and two simulate a large expansion of the OMZ that reinforce the expansion in the thermocline (IPSL-CM6A-LR, CNRM-ESM2-1, Figure 3d). The OMZ contraction in the first two models (MRI-ESM2-0 and ACCESS-ESM1-5) is, however, associated with a strong and unlikely collapse in primary productivity in the future (Figure B2), which could impede their ability to project future OMZ changes in intermediate waters. The two other models (IPSL-CM6A-LR, CNRM-ESM2-1) simulate an unrealistic historical OMZ extent, suggesting significant biases in the physical

and biological processes controlling O_2 in their OMZ (see FigureA1 panels e and c). Although the peculiar behavior of these four ESMs contributes to the uncertainty in the future response of the OMZ, the ESM ensemble robustly project an expansion of the Pacific OMZ, controlled by the O_2 changes in the thermocline and partially offset by the O_2 changes in intermediate waters (Figure 2d/e).

3.3 Weaker subtropical overturning controls robust OMZ expansion in thermocline

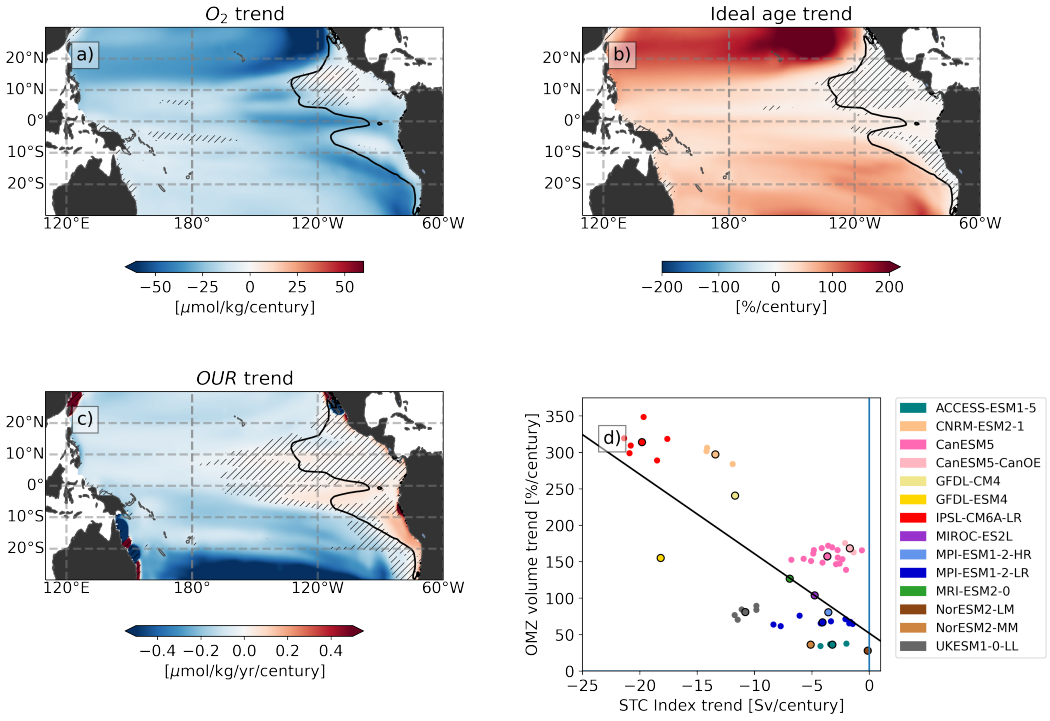

Figure 4: Mechanisms controlling the OMZ expansion in the thermocline. Changes in **a)** O_2 (14 ESMs median), **b)** ideal tracer age (10 ESMs median) and **c)** oxygen utilization rate (OUR) (10 ESMs median). Changes are computed as linear trends over yearly data from 2000 to 2100 using historical and SSP5-8.5 experiments and shown as multi-ESM median. Hatching indicates where less than 75% of the ESMs agree with the sign of the model median. d) Relationship between changes in OMZ volume and subtropical cell index (STCI, the strength of meridional transport by subtropical cell, see Methods) in CMIP6 ESMs (individual members are indicated by smaller symbols).

The robust expansion of the OMZ simulated in the thermocline is associated with a widespread loss of O_2 in the tropical Pacific Ocean in that density layer (multi-ESM median loss of -23 $\mu mol/kg$ from 2000-2100 average across the tropical Pacific; Figure 4a). This loss is strongest along the ventilation pathways that flank the OMZ and is concomitant with an increase of about 76 % in ideal age tracer over the basin (the time since the watermass was last in contact with the atmosphere increases, Figure 4b). This suggests that the OMZ expansion in the thermocline is caused by a basin-scale weakening of the ocean circulation and not by localized changes or redistribution of O_2 within the OMZ.

To examine the potential role of biological activity, we are using oxygen utilization rate OUR (see Methods). While the decrease in ideal age is consistent with the sign of O_2 changes in the domain, changes in OUR are only consistent locally. ESMs consistently project a decline in OUR in the thermocline outside of the OMZ and near-neutral changes within the OMZ (Figure 3c). This reduced O_2 biological demand is consistent with the decline in export production simulated in most ESMs (Figure B2) but is not consistent with the projected change in O_2 (reduced OUR alone would increase O_2). Biological processes thus act to offsets part of the weaker supply of O_2 by ventilation and act as stabilizing feedback on O_2 levels and the OMZ in the thermocline. This result is in line with prior work that showed that increased stratification and weaker eddy turbulent mixing associated with global warming reduced the upward transport of nutrients that fuel biological production and O_2 consumption at depth (Deutsch et al., 2014; Duteil et al., 2014; Doney & Karnauskas, 2014; Duteil et al., 2018; Palter & Trossman, 2018; Couespel et al., 2019). OUR only provides a qualitative assessment of changes in biological demand and is strongly limited in regions where mixing dominates the ocean transport, such as the OMZ core (Koeve & Kähler, 2016). As a result, we cannot quantify the magnitude of the compensation between ventilation changes and biogeochemical feedback in the ESMs examined here (which would require a detailed O_2 budget). The very robust and consistent OMZ expansion and largescale O_2 decline projected by all ESMs strongly suggests, however, that the biogeochemical feedback is small compared to the weakening of the subtropical overturning in the thermocline (Figure 3).

To establish the link between deoxygenation and ventilation changes in the thermocline, we use the Subtropical Cell Index (STCI; the difference between the maxima/minima of the overturning streamfunction between 10°S-10°N in the upper 250 m) as an indicator of the strength of the Subtropical cells that transport oxygenated waters from the subtropics (approx 30°S and 30°N) to the OMZ (see Methods). The expansion of the OMZ in the thermocline is tightly linked to the weakening of the subtropical cells simulated by the ESMs, with an average $11 \pm 3\%$ increase in OMZ volume for a decrease of 1 Sv in the STCI (Figure 3c). This result is consistent with the work of Duteil et al. (2014) who identified a strong link between changes in upper ocean O_2 and shallow overturning circulation in the tropical Pacific Ocean since the 1960s using an ocean bio-physical model. The key role of large-scale circulation is further supported by the fact that the rate of OMZ expansion depends on the ESM but only marginally depends on the choice of the O_2 threshold used to define the OMZ boundary. For instance, the OMZ volume increases by ∼30 % in NorESM2-MM and by ∼50 % in MPI-ESM1-2-LR whether we use 10, 80 or 120 $\mu mol/kg$ to define the OMZ (Figure C1). This suggests that the basin-scale decline in O_2 attributed to reduced subtropical advection propagates to the OMZ in the shadow zones by slow mixing processes.

3.4 Biogeochemical feedbacks and near-neutral OMZ changes in intermediate waters

The relatively weak OMZ volume changes projected in intermediate waters (Figure 3d) are caused by the compensation between changes in ocean circulation and biological demand. We illustrate this compensation using four ESMs (CanESM5, CanESM5-CanOE, GFDL-CM4, and GFDL-ESM4) that simulate a total OMZ historical volume (thermocline + intermediate waters) within 35% of observations (Figure 1g). CanESM5 and CanESM5-CanOE are identical except for the ocean biogeochemical module that is more complex in CanESM5-CanOE (Swart et al., 2019a). Interpretation of the comparison between GFDL's CM4 and ESM4 is not as straightforward, since both setups differ by the complexity of the ocean biogeochemistry (BLINGv2 (Dunne, Bociu, et al., 2020) vs. COBALTv2 (Stock et al., 2020)) but also by the configuration of the ocean, atmosphere, and land, such as the horizontal ocean resolution which is lower in ESM4 (nominal 1/2 degree with eddy scale thickness mixing parameterization) than in CM4 (nominal 1/4 degree, Dunne, Horowitz, et al. (2020) without an eddy parameterization).

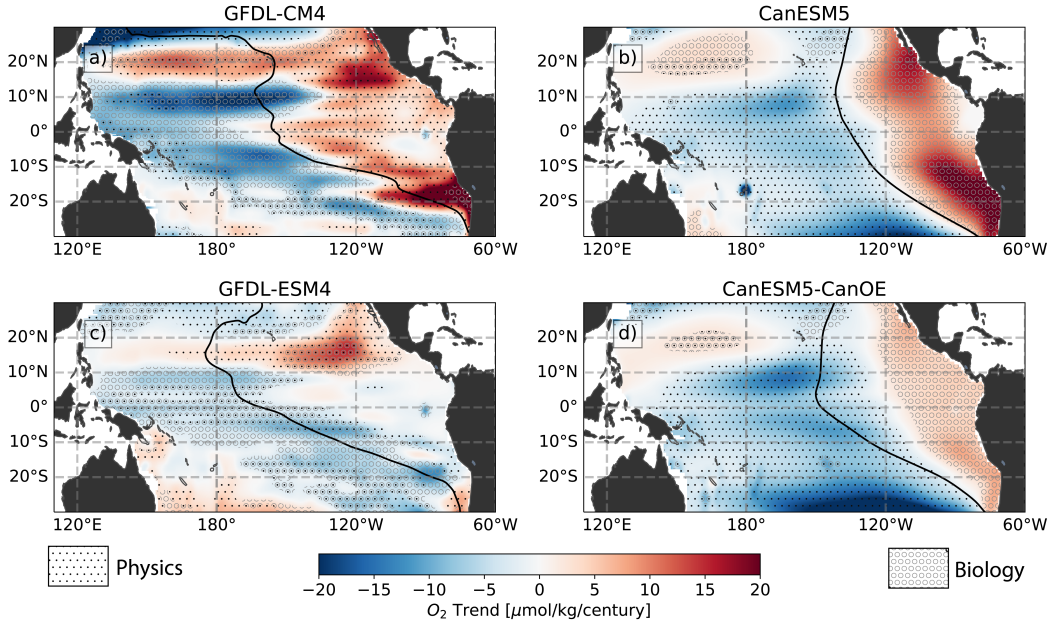

Figure 5: Mechanisms controlling the OMZ expansion in the intermediate waters in four ESMs, two with simpler (upper row) and two with more complex (lower row) marine biogeochemical modules. Changes in mean O_2 in the intermediate waters layer (colors) and the historical (1960-2000 average) OMZ boundary (black contours) are shown. Hatching types indicate if physical, biological, or both control the O_2 changes: small black dots indicate O_2 changes consistent with the sign of change in ideal age (physical driver), open grey circles show agreement between O_2 and OUR changes (biological driver). Regions consistent with both age and OUR changes are marked by both symbols. Areas with O_2 changes smaller than $2\mu mol/kg/century$ are not hatched for clarity. All fields are smoothed with a ~ 1 degree Gaussian filter before plotting.

The four ESMs project changes in OMZ volume between approximately $-3\times10^{15}m^3$ and $1\times10^{15}m^3$ $10^{15}m^3$ in the intermediate waters check again Figure 2). The O_2 changes in this layer have similar spatial patterns in the four ESMs, but the mechanisms that control these changes are different (Figure 5). The four ESMs simulate a decline in O_2 outside and along the OMZ boundary and an increase in O_2 at least in some part of the OMZ core (Figure 5). O_2 changes are more spatially variable in the two GFDL models, likely due to their higher horizontal resolution (1 degree for CanESM vs. 1/2 to 1/4 degree for GFDL models), the lack of eddy thickness mixing parameterization in CM4, and the lower number of members available to isolate the forced signal from natural variability (3 to 17 members for CanESM ESMs vs. one member for GFDL; Table 1). Notably, the increase in O_2 in the OMZ core is more intense and widespread in ESMs with simpler biogeochemical modules (CanESM5, GFDL-CM4) than in the more complex ESMs (CanESM5-CanOE, GFDL-ESM4).

In Figure 5, we examine whether ventilation changes (using ideal age), biological changes (using OUR), or both are consistent with the sign of O_2 changes. In both CanESM5 models, reduced O_2 outside and along the edges of the OMZ are consistent with older ages and inconsistent with lower OUR (Figure 5 b and d), indicating that weaker basin-scale ventilation controls the O_2 loss in the intermediate waters in these two ESMs (Figure 5 b and d). In contrast, large regions of reduced O_2 levels in the two GFDL ESMs are consistent with higher OUR but inconsistent with younger simulated ages, suggest-

ing that changes in biological respiration are a primary control of the O_2 loss in these ESMs (Figure 5 a and c). Within the OMZ, O_2 changes are very similar in both CanESM ESMs and consistent with reduced respiration (less OUR), while in the GFDL ESMs, they are consistent with a combination of changes in respiration and ventilation by mixing processes (Figure 5). We note that our analysis relies on a rough consistency check between the sign of O_2 change and OUR/ideal age, and their interpretation becomes difficult in regions not dominated by strong advection (Koeve & Kähler, 2016). The O_2 changes attributed to the combination of biological and physical processes in the GFDL ESMs could therefore be controlled by mixing (mixing could influence OUR via the apparent oxygen utilization without the need for respiration changes).

These four ESMs offer the opportunity to compare the OMZ change between pairs of ESMs with very similar architecture but different biogeochemical modules. These ESMs respond differently, yet they suggest that the OMZ volume in the intermediate waters is relatively stable because of the balance between physical and biological changes. In both ESM pairs, the more complex biogeochemical module leads to a weaker O_2 increase within the OMZ core and less contraction of the OMZ (Figure 3d). This suggests that additional biogeochemical feedbacks represented in these ESMs likely offset the oxygenation of the OMZ core controlled by either ventilation (mixing changes) or by the respiration feedback (less export production leads to less oxygen respiration) and act to stabilize the OMZ. For instance, denitrification, which is represented in the two more complex modules (switch to nitrate-based respiration at low oxygen levels in GFDL-ESM4 (Stock et al., 2020) and CanESM-CanOE (Swart et al., 2019a)) could buffer O_2 changes in the OMZ core (Lachkar et al., 2016).

4 Conclusions

We used the latest CMIP6 ESM generation to investigate the future evolution of the Pacific OMZ. The results show that climate change under high greenhouse gas emissions will very likely lead to an expansion of the OMZ in the tropical Pacific by the end of the 21st century. The expansion is controlled by decreased ventilation of the thermocline, while changes in intermediate waters modulate the magnitude of the expansion. The robustness of these results across various ESMs stands in contrast to prior work that showed no consistent projections in the Pacific (Cabré et al., 2015; Shigemitsu et al., 2017; Bopp et al., 2013; Kwiatkowski et al., 2020).

Differences between our results showing robust OMZ expansion and prior findings can be explained by two factors. First, the representation of the OMZ has improved in many ESMs compared to the prior generation of ESMs used in most of these studies (Cabré et al., 2015; Shigemitsu et al., 2017; Bopp et al., 2013), specifically the representation of the Equatorial current system (Karnauskas et al., 2020) which strongly affect the historical extent of the upper OMZ (J. J. M. Busecke et al., 2019). The crucial role of ventilation changes highlighted here strongly suggests that a better representation of the OMZ hinges on better constraints of the transport pathways from the subtropics and mid-latitude into the Tropical Pacific.

Second, our approach crucially relies on the analysis of the OMZ in a density framework. When analyzing the OMZ in depth space, biases and changes in stratification in different ESMs lead to an arbitrary separation of the different dynamical regimes that shape the OMZ that hinder the interpretability of results. This is illustrated in Figure 6 where we compare the change in volume in the 14 CMIP6 ESMs using a depth framework vs. using the density framework we proposed here. The depth framework leads to inconclusive OMZ volume changes, similar to what was found in earlier studies (Cabré et al., 2015; Shigemitsu et al., 2017; Bopp et al., 2017; Kwiatkowski et al., 2020). In this framework, the consistent expansion of the OMZ in the thermocline is arbitrarily accounted for in the shallow (0-1000m) or split between the shallow and mid-depth (1000-2000m)

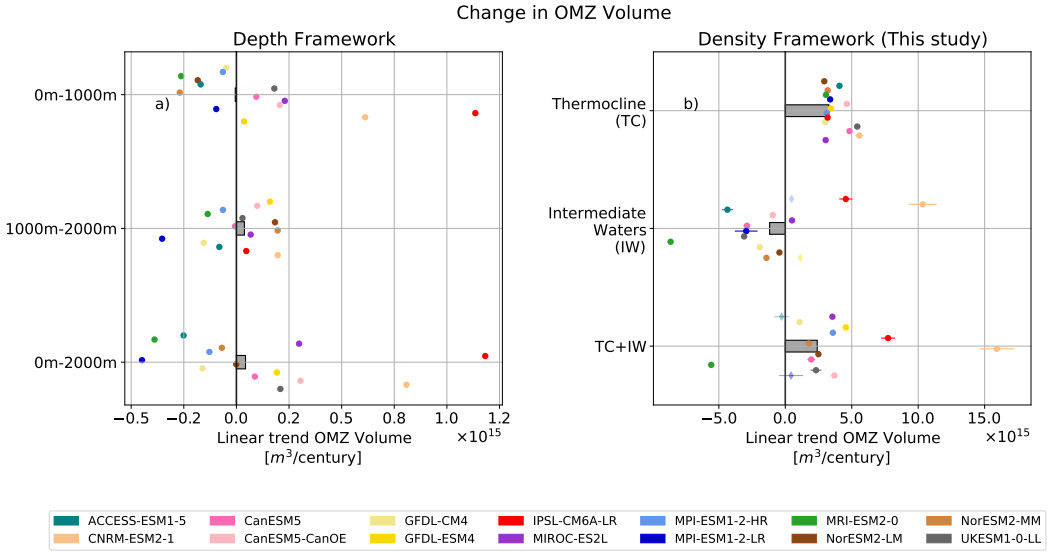

Figure 6: Change in OMZ volume in the 14 ESMs using **a)** a constant depth framework and **b)** a constant density framework (same as Figure3d). Changes are computed using linear trends from 2000 to 2100. Values in a) are only shown for a single member for illustration purposes. Grey bar indicates Multi-ESM median.

layers depending on the model. Similarly, intermediate waters can be fully accounted for in the mid-depth layer, be split between the shallow and mid-depth layer, or even have a part that extends deeper and is not accounted for. Note that the choice of the depths (surface, 1000m, and 2000m here) has little influence on this finding. In contrast, the density framework shows changes that are more robust in their sign and amplitude (Figure 6b). These results suggest that the density framework used here might be able to partially reconcile the discrepancies found in older model generations as well.

We note two caveats in the projection of the Pacific OMZ expansion. The ESMs agree very well in the thermocline, but the uncertain balance between physical and biological effects in the intermediate waters introduces uncertainties in the magnitude of the OMZ expansion. Depending on the ESM, the robust changes in the thermocline can be modulated by OMZ contraction/expansion in the intermediate waters. While the multi-model median suggests a near-zero change or a slight contraction of the OMZ in intermediate waters, further work is needed to determine the magnitude of this change. In addition, we note that, unlike in observations, 10 out of 14 ESMs simulate hypoxic waters in deep waters below the intermediate waters, at depth that often exceeds 2000 m (Figure A2 and Figure A3). Most of these ESMs show a contraction of the OMZ volume in the deep ocean. In this study, however, we focused on the thermocline and intermediate layers where the OMZ is found in nature and excluded these unrealistic deep OMZs ventilated by denser water masses on longer timescales (Heuzé (2020)), which have therefore less relevance to understanding the future of the Pacific OMZ.

Our results suggest that biogeochemical feedbacks might be important for the OMZ volume in the intermediate waters and hence the magnitude of the total OMZ expansion (both in the thermocline and intermediate waters). Specifically, in the ESM case studies presented here, we find that ESMs with higher complexity in the biogeochemical module (GFDL-ESM4 vs. GFDL-CM4 and CanESM5-CanOE vs. CanESM5) show smaller changes in OMZ volume in the intermediate waters, compared to their simpler biogeochemical counterparts (noting that for the GFDL ESMs the comparison is less clear

ESM	Variables	Number of Members
ACCESS-ESM1-5 (Ziehn et al., 2019a, 2019b)	agessc, epc100, mlotst, o2, so, thetao, vo	3
CNRM-ESM2-1 (Seferian, 2018, 2019)	epc100, mlotst, o2, so, thetao, vo	5
CanESM5 (Swart et al., 2019d, 2019e)	agessc, epc100, mlotst, o2, so, thetao, vo	17
CanESM5-CanOE (Swart et al., 2019b, 2019c)	agessc, epc100, mlotst, o2, so, thetao, vo	3
GFDL-CM4 (Guo et al., 2018a, 2018b)	agessc* (yr), o2 (gr), so, thetao, vo	1
GFDL-ESM4 (Krasting et al., 2018; John et al., 2018)	agessc* (yr), epc100 (gr), mlotst, o2 (gr), so, thetao, vo*	1
IPSL-CM6A-LR (Boucher et al., 2018, 2019)	agessc, epc100, mlotst, o2, so, thetao, vo	6
MIROC-ES2L (Hajima et al., 2019; Tachiiri et al., 2019)	agessc, epc100, o2, so, thetao, vo	1
MPI-ESM1-2-HR (Jungclaus et al., 2019; Schupfner et al., 2019)	epc100, mlotst, o2, so, thetao, vo	2
MPI-ESM1-2-LR (Wieners et al., 2019a, 2019b)	agessc, epc100, mlotst, o2, so, thetao, vo	10
MRI-ESM2-0 (Yukimoto et al., 2019a, 2019b)	epc100, mlotst, o2, so, thetao, vo	1
NorESM2-LM (Seland et al., 2019a, 2019b)	agessc (gr), epc100, mlotst, o2 (gr), so (gr), thetao (gr), vo	1
NorESM2-MM (Bentsen et al., 2019a, 2019b)	agessc (gr), epc100, mlotst, o2 (gr), so (gr), thetao (gr), vo	1
UKESM1-0-LL (Tang et al., 2019; Good et al., 2019)	epc100, mlotst, o2, so, thetao, vo	1

Table 1: ESM data used in this study. Variables used: Dissolved oxygen concentration (o2), salinity (so), potential temperature (thetao), mixed layer depth (mlotst), particulate carbon export at 100 m (epc100), and ideal age (agessc) where available. We only use members that provide all data and can be detrended (some members could not be detrended due to errors in the metadata). The number of members used here can therefore be lower than the number published by the modeling center on ESGF). If not otherwise marked variables are given as monthly averages on the native ocean grid of the respective ESM. Variables with 'gr' were only available as regridded 1° by 1° outputs and have been bilinearly interpolated on the native grid. Variables with 'yr' were only available as yearly output and were interpolated linearly to monthly intervals before analysis. Variable marked with an asterisk (*) are not available via ESGF and were provided by GFDL collaborator Jasmin John.

since the physical setup also differs). A more in-depth analysis of these feedbacks would be needed to quantify their magnitude. If the importance of biogeochemical feedbacks is confirmed, realistic future expansion of the Pacific OMZ would depend mostly on the response in the thermocline and lie in the upper range of the values analyzed here (i.e., $3.5 - 5 \times 10^{15} m^3$).

The increase in OMZ thickness, and particularly the expansion of the OMZ in the thermocline in response to anthropogenic forcing, will translate into a shallowing of the upper boundary of the OMZ. This shallowing of low oxygenated waters would maximize the detrimental ecological and economic consequences since the upper boundary of the OMZ has a disproportionate effect on ecosystems, ecosystem services such as fisheries (Stramma et al., 2012), and greenhouse gas (N_2O) emissions (Yang et al., 2017) with positive feedback on the Earth System.

Appendix A Historical OMZ distribution in individual ESMs

The spatial extent of the OMZ is different in all ESMs (Figure A1 and A2). Three ESMs, in particular, show an OMZ extent that strongly differs from observations, likely impeding their ability to project future changes. The OMZ in CNRM-ESM2-1 is too large, with hypoxic waters extending over the whole basin up to the western boundary and all the way to the ocean floor into deeper waters (Figs A1 and A2 panels b). In contrast, IPSL-CM6A-LR shows very little hypoxic waters in the thermocline and intermediate waters, except very near the eastern Pacific coasts (Figs. A1 and A2 panels g). MIROC-ES2L shows the smallest OMZ of all ESMs (Figs. A1 and A2 panels h), largely underestimating its volume (Figure 1g) . Additionally, this ESM has strong biases in the wa-

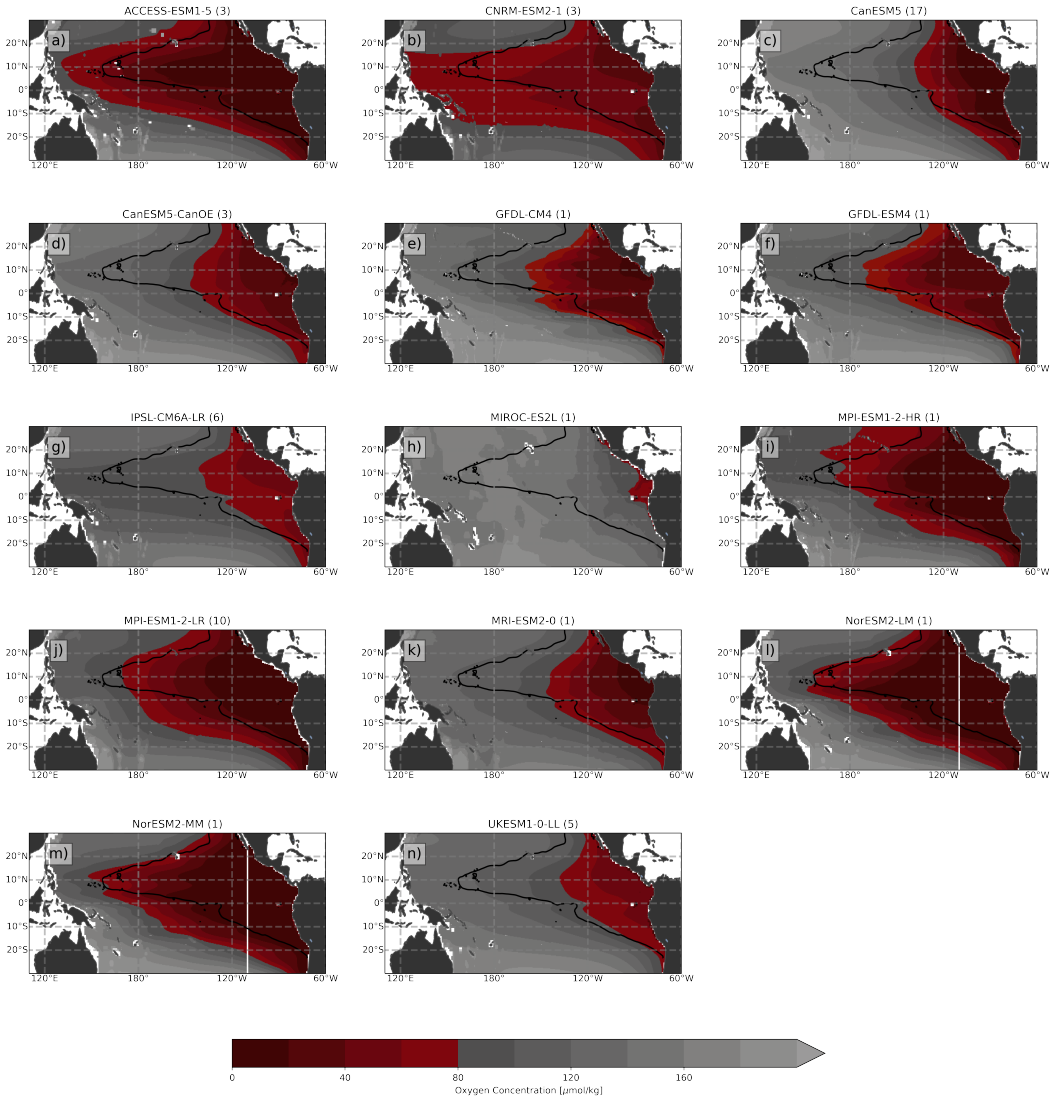

Figure A1: O_2 concentrations averaged over thermocline and intermediate waters (same as Figure 1b) for each ESM used in this study. Where appropriate ESM members are averaged. Black contour shows the 80 $\mu mol/kg$ contour from World Ocean Atlas observations (see Figure 1a).

ter column stratification; there are no very dense waters in this model (note the $sigma_0 = 27.65$ line does not exist in Figure A2 h). In these three models, biases in the ocean circulation and ventilation are likely responsible for the misrepresentation of the historical OMZ extent and their potentially unrealistic projections of OMZ volume in the future (Figure 3).

In this study, we focused on the thermocline and intermediate layers, excluding the 'deep' density layer where only a small proportion of the observed OMZ (about 0.3%) is present in our region of interest (Tropical Pacific 30°S-30°N; for details, see Methods). Many of the ESMs, however, simulate a deeper OMZ at depth that often exceeds 2000 m (Figure A2 and Figure A3). These unrealistic deep OMZs are ventilated by different

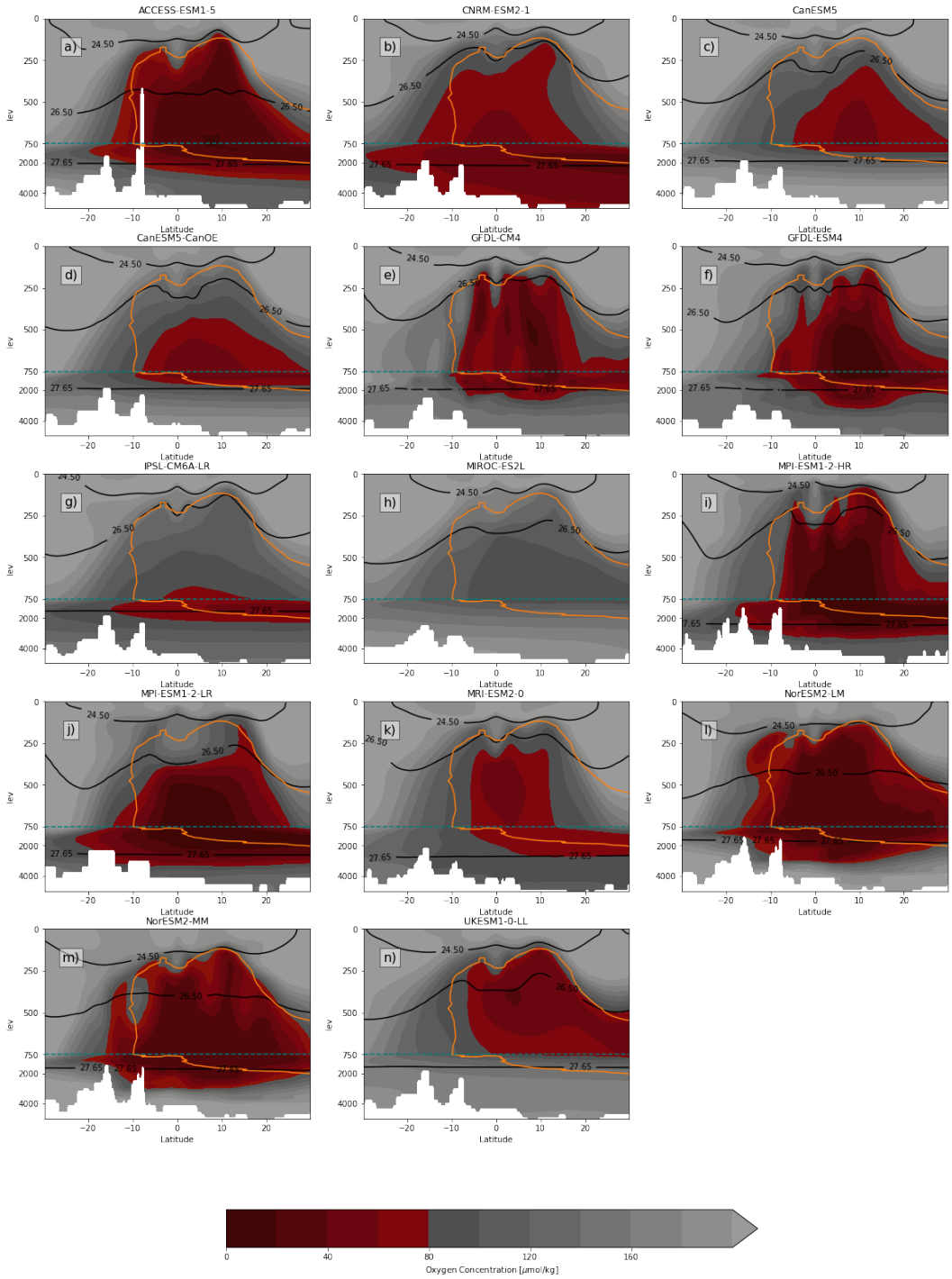

Figure A2: O_2 concentrations along a depth section at 140°W (same as Figure 1d) for each ESM used in this study. Orange contour shows the 80 μmol/kg contour from World Ocean Atlas observations (see Figure 1a). Black contour shows the $sigma_0$ boundaries used to delimit thermocline and intermediate waters.

water masses and on different timescales than the OMZ found in nature and have therefore little relevance to understanding the future of the Pacific OMZ.

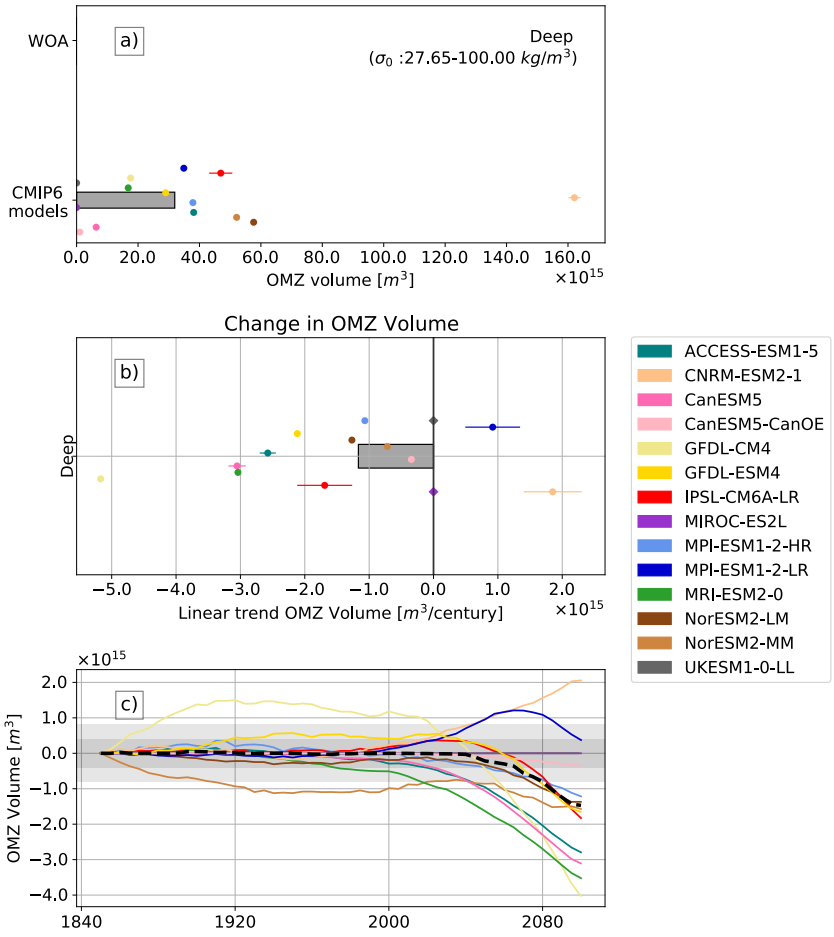

Figure A3: **a)** OMZ volume during the historical period and trends over 2000-2100 period for the deep ocean ($\sigma_0 > 27.65\,kg/m^3$) for World Ocean Atlas observations and 14 CMIP6 ESMs. **a)** Historical OMZ volume for Observations and ESMs Same as Figure 1 e-g for deep ocean. **b)** Linear trend in OMZ volume for CMIP6 ESMs. Same as Figure 3d for deep ocean. **c)** Timeseries of OMZ volume for CMIP6 ESMs. Same as Figure 3 a/b for deep ocean.

Appendix B Simulated changes in OMZ thickness and carbon export in individual models

The changes in OMZ thickness are very consistent between all the ESMs but depend on the historical extent of the OMZ (indicated as black contours in Figure B1). For instance, both CanESM5-CanOE (Figure B1e) and MPI-ESM1-2-LR (Figure B1k) both show increases in OMZ thickness, but the changes in CanESM5-CanOE are much more confined to the eastern basin, similarl to the historical OMZ in those models.

The historical particulate carbon export at 100m depth is markedly lower compared to CMIP5 estimates (compare to Cabré et al. (2015) Figure 5), and with values between 0.4-1.2 Pg/yr closer to observational estimates by Siegel et al. (2014) and Dunne et al. (2005), but still considerably larger than estimates by Henson et al. (2012). Most models simulate a decline of export at the end of the century. 12 out of the 13 ESMs which provided export output show a decline in particulate export ranging from 5% to over 30% compared to the historical period (Figure B2). The particulate carbon export declines

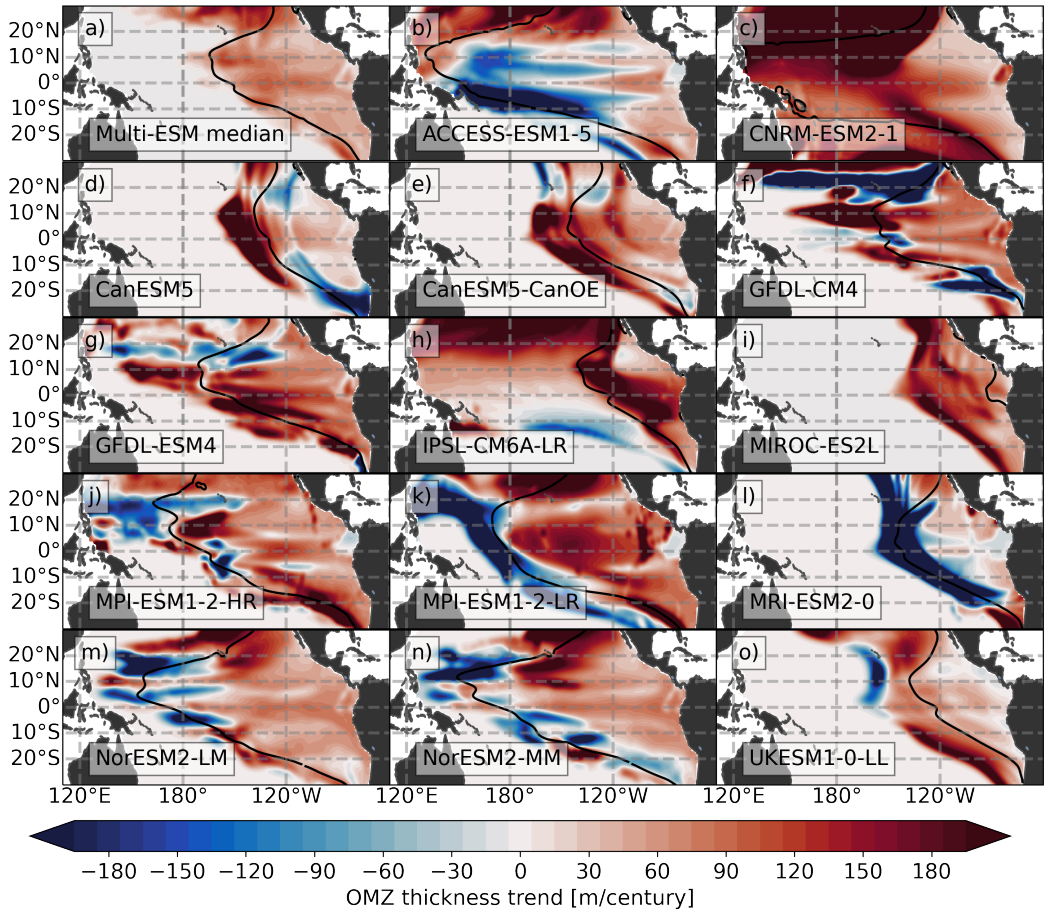

Figure B1: Changes in OMZ thickness computed as the linear trend from 2000-2100 in thermocline+intermediate waters **a)** Multi-ESM median (same as Figure 2) and each individual ESM (members averaged when available). All fields are smoothed with ∼1 degree gaussian kernel and OMZ historical extent is indicated by contour (80 μmol/kg).

very strongly in two ESMs (ACCESS-ESM1-5 and MRI-ESM2-0, Figure B2), which also show a strong decline in OMZ volume in the intermediate waters from 2000 to 2100 (Figure 3b). Emergent constraints on the decline in primary productivity suggest that such extreme changes in carbon export and the associated oxygen demand at depth are rather unlikely (Kwiatkowski et al., 2017), and that the strong decrease in OMZ volume simulated in these models might not be realistic.

Appendix C Robustness of OMZ projection in density framework

In the main manuscript, we use a unique threshold of 80 $\mu mol/kg$ to define the OMZ. Figure C1 shows however, that the results are largely insensitive to the choice of the oxygen threshold, in particular in the thermocline. This suggests that changes in OMZ volume in the thermocline are driven by large basin-scale changes in O_2 concentrations and not localized changes (these would only affect some of the thresholds). It also shows how our density framework adds to the robustness of the multi-ESM projection compared to prior work using depth layers. For instance Bopp et al. (2013); Cabré et al. (2015) showed that both the sign and magnitude of the projected OMZ volume change depended on

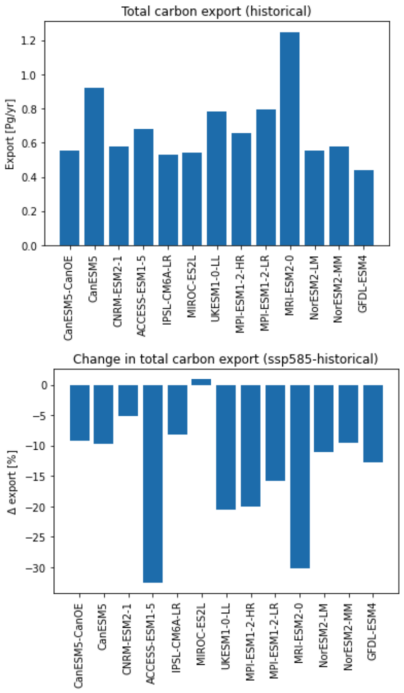

Figure B2: Particulate organic carbon export at 100 m depth (variable epc100) for 20°S-20°N and 180°W-60°W. **Upper**: Historical export (1960-2000) **Lower**: Percent change of export from 2060-2100 to 1960-2000.

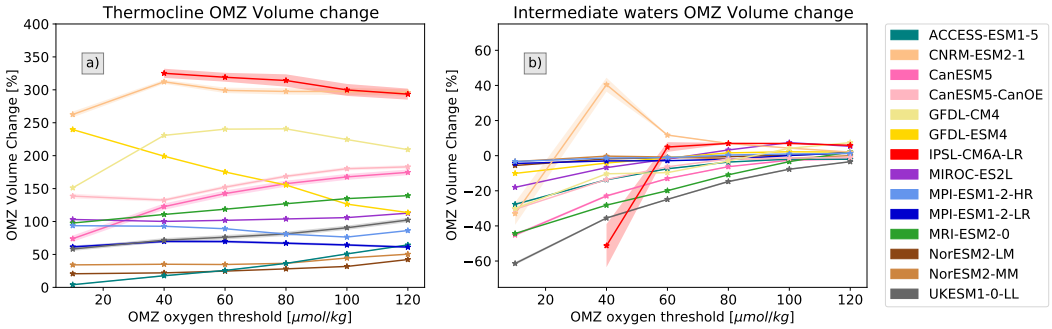

Figure C1: Change in OMZ volume for various O_2 thresholds in the thermocline (a) and intermediate waters (b). Values are calculated as the linear trend over yearly data from 2000-2100 relative to the 1960-2000 OMZ volume (only shown if 1960-2000 OMZ volume exceeds $5 \times 10^{13}\, m^3$). Shading indicates ±1 standard deviation of the ESM members when available.

the O_2 threshold (note that only Cabré et al. (2015) isolates changes for the Pacific ocean). See details in the conclusion of the main text.

Acronyms

OMZ Oxygen Minimum Zone
ESM Earth System Model

AOU Apparent Oxygen Utilization
OUR Oxygen Utilization Rate
STCI Subtropical Cell Index

Acknowledgments

The study has been supported by the Cooperative Institute for Modeling the Earth System between NOAA GFDL and Princeton University, the High Meadows Environmental Institute CMI, and the Sloan Foundation. We acknowledge the World Climate Research Programme, which, through its Working Group on Coupled Modelling, coordinated and promoted CMIP6. We thank the climate modeling groups for producing and making available their model output, the Earth System Grid Federation (ESGF) for archiving the data and providing access, and the multiple funding agencies who support CMIP6 and ESGF. The authors thank the pangeo project (R. P. Abernathey et al., 2021) and their cloud computing/storage resources, which were used for prototyping and software development. The code to reproduce our results is provided in a zenodo archive(`https://zenodo.org/record/4742926`). Processed data files, used to create plots are available in another zenodo archive (`https://sandbox.zenodo.org/record/812722#.YJV31i9h2wI`). J.B. led the analysis of the CMIP results and prepared the figures. J. J. provided additional model outputs for GFDL-CM4 and GFDL-ESM4. J.B. and L. R. designed this study, interpreted the results, and wrote the manuscript. The authors thank John P. Dunne for his thorough review of the study.

References

Abernathey, R. (2021, February). *xgcm/fastjmd95: v0.2.1.* Zenodo. Retrieved from `https://doi.org/10.5281/zenodo.4498376` doi: 10.5281/zenodo.4498376

Abernathey, R., Busecke, J., Smith, T., Bot, S., Banihirwe, A., Zhang, C., ... Rath, W. (2020, October). *xgcm/xgcm: v0.5.1.* Zenodo. Retrieved from `https://doi.org/10.5281/zenodo.4097223` doi: 10.5281/zenodo.4097223

Abernathey, R. P., Augspurger, T., Banihirwe, A., Blackmon-Luca, C. C., Crone, T. J., Gentemann, C. L., ... Signell, R. P. (2021). Cloud-native repositories for big scientific data. *Computing in Science Engineering*, *23*(2), 26–35.

Babbin, A. R., Bianchi, D., Jayakumar, A., & Ward, B. B. (2015). Rapid nitrous oxide cycling in the suboxic ocean. *Science*, *348*(6239), 1127–1129.

Bahl, A., Gnanadesikan, A., & Pradal, M.-A. (2019). Variations in ocean deoxygenation across earth system models: Isolating the role of parameterized lateral mixing. *Global Biogeochemical Cycles*, *33*(6), 703–724.

Banihirwe, A., Long, M., bonnland, Kent, J., Spring, A., Busecke, J., ... Paul, K. (2020, November). *intake/intake-esm: Intake-esm v2020.11.4.* Zenodo. Retrieved from `https://doi.org/10.5281/zenodo.4243421` doi: 10.5281/zenodo.4243421

Bentsen, M., Oliviè, D. J. L., Seland, y., Toniazzo, T., Gjermundsen, A., Graff, L. S., ... Schulz, M. (2019a). *Ncc noresm2-mm model output prepared for cmip6 cmip.* Earth System Grid Federation. Retrieved from `https://doi.org/10.22033/ESGF/CMIP6.506` doi: 10.22033/ESGF/CMIP6.506

Bentsen, M., Oliviè, D. J. L., Seland, y., Toniazzo, T., Gjermundsen, A., Graff, L. S., ... Schulz, M. (2019b). *Ncc noresm2-mm model output prepared for cmip6 scenariomip.* Earth System Grid Federation. Retrieved from `https://doi.org/10.22033/ESGF/CMIP6.608` doi: 10.22033/ESGF/CMIP6.608

Bertrand, A., Chaigneau, A., Peraltilla, S., Ledesma, J., Graco, M., Monetti, F., & Chavez, F. (2011). Oxygen: a fundamental property regulating pelagic ecosystem structure in the coastal southeastern tropical pacific. *PLoS One*, *6*(12), e29558.

Bopp, L., Resplandy, L., Orr, J. C., Doney, S. C., Dunne, J. P., Gehlen, M., ... Vichi, M. (2013). Multiple stressors of ocean ecosystems in the 21st century: projections with cmip5 models. *Biogeosciences*, 21.

Bopp, L., Resplandy, L., Untersee, A., Le Mezo, P., & Kageyama, M. (2017). Ocean (de)oxygenation from the last glacial maximum to the twenty-first century: insights from earth system models. *Philosophical Transactions of the Royal Society A: Mathematical, Physical and Engineering Sciences*, *375*(2102), 20160323.

Boucher, O., Denvil, S., Levavasseur, G., Cozic, A., Caubel, A., Foujols, M.-A., ... Cheruy, F. (2018). *Ipsl ipsl-cm6a-lr model output prepared for cmip6 cmip.* Earth System Grid Federation. Retrieved from `https://doi.org/10.22033/ESGF/CMIP6.1534` doi: 10.22033/ESGF/CMIP6.1534

Boucher, O., Denvil, S., Levavasseur, G., Cozic, A., Caubel, A., Foujols, M.-A., ... Lurton, T. (2019). *Ipsl ipsl-cm6a-lr model output prepared for cmip6 scenariomip.* Earth System Grid Federation. Retrieved from `https://doi.org/10.22033/ESGF/CMIP6.1532` doi: 10.22033/ESGF/CMIP6.1532

Busecke, J., & Spring, A. (2020, April). *jbusecke/cmip6_preprocessing: v0.1.4.* Zenodo. Retrieved from `https://doi.org/10.5281/zenodo.3743397` doi: 10.5281/zenodo.3743397

Busecke, J. J. M., Resplandy, L., & Dunne, J. P. (2019). The equatorial undercurrent and the oxygen minimum zone in the pacific. *Geophysical Research Letters Geophys. Res. Lett.*, *46*(12), 6716–6725.

Cabré, A., Marinov, I., Bernardello, R., & Bianchi, D. (2015). Oxygen minimum zones in the tropical pacific across cmip5 models: mean state differences and climate change trends. *Biogeosciences*, *12*(18), 5429–5454.

Chavez, F. P., Bertrand, A., Guevara-Carrasco, R., Soler, P., & Csirke, J. (2008). The northern humboldt current system: Brief history, present status and a view towards the future. *Progress in Oceanography*, *79*(2-4), 95–105.

Couespel, D., Lévy, M., & Bopp, L. (2019). Major contribution of reduced upper ocean oxygen mixing to global ocean deoxygenation in an earth system model. *Geophysical Research Letters*, *46*(21), 12239–12249.

Deutsch, C., Berelson, W., Thunell, R., Weber, T., Tems, C., McManus, J., ... Geen, A. v. (2014). Centennial changes in north pacific anoxia linked to tropical trade winds. *Science*, *345*(6197), 665–668.

Doney, S. C., & Karnauskas, K. B. (2014). Oxygen and climate dynamics. *Nature Climate Change*, *4*(10), 862–863.

do Rosário Gomes, H., Goes, J., Matondkar, S., Buskey, E., Basu, S., Parab, S., & Thoppil, P. (2014). Massive outbreaks of noctiluca scintillans blooms in the arabian sea due to spread of hypoxia. *Nat Commun*, *5*, 4862.

Dunne, J. P., Armstrong, R. A., Gnanadesikan, A., & Sarmiento, J. L. (2005). Empirical and mechanistic models for the particle export ratio. *Global Biogeochemical Cycles*, *19*(4), n/a–n/a.

Dunne, J. P., Bociu, I., Bronselaer, B., Guo, H., John, J. G., Krasting, J. P., ... Zadeh, N. (2020). Simple global ocean biogeochemistry with light, iron, nutrients and gas version 2 (blingv2): Model description and simulation characteristics in gfdl's cm4.0. *Journal of Advances in Modeling Earth Systems*, *12*(10).

Dunne, J. P., Horowitz, L. W., Adcroft, A. J., Ginoux, P., Held, I. M., John, J. G., ... Zhao, M. (2020). The gfdl earth system model version 4.1 (gfdl-esm 4.1): Overall coupled model description and simulation characteristics. *Journal of Advances in Modeling Earth Systems*, *12*(11).

Duteil, O., Böning, C. W., & Oschlies, A. (2014). Variability in subtropical-tropical cells drives oxygen levels in the tropical pacific ocean. *Geophysical Research Letters*, *41*(24), 8926–8934.

Duteil, O., & Oschlies, A. (2011). Sensitivity of simulated extent and future evo-

lution of marine suboxia to mixing intensity. *Geophysical Research Letters*, *38*(6), n/a–n/a.

Duteil, O., Oschlies, A., & Böning, C. W. (2018). Pacific decadal oscillation and recent oxygen decline in the eastern tropical pacific ocean. *Biogeosciences Discussions*, 1–30.

Eyring, V., Bony, S., Meehl, G. A., Senior, C. A., Stevens, B., Stouffer, R. J., & Taylor, K. E. (2016). Overview of the coupled model intercomparison project phase 6 (cmip6) experimental design and organization. *Geoscientific Model Development*, *9*(5), 1937–1958.

Firing, E., Filipe, Barna, A., & Abernathey, R. (2021, Mar). *Teos-10/gsw-python: v3.4.1.* Zenodo. Retrieved from `https://doi.org/10.5281/zenodo.4631364` doi: 10.5281/zenodo.4631364

Frölicher, T. L., Aschwanden, M. T., Gruber, N., Jaccard, S., Dunne, J. P., & Paynter, D. (2020). Contrasting upper and deep ocean oxygen response to protracted global warming. *Global Biogeochemical Cycles*.

Garcia, H. E., Boyer, T. P., Locarnini, R. A., Antonov, J. I., Mishonov, A. V., Baranova, O. K., ... Levitus, S. (2013). World ocean atlas 2013. volume 3, dissolved oxygen, apparent oxygen utilization, and oxygen saturation.

Good, P., Sellar, A., Tang, Y., Rumbold, S., Ellis, R., Kelley, D., ... Walton, J. (2019). *Mohc ukesm1.0-ll model output prepared for cmip6 scenariomip.* Earth System Grid Federation. Retrieved from `https://doi.org/10.22033/ESGF/CMIP6.1567` doi: 10.22033/ESGF/CMIP6.1567

Guo, H., John, J. G., Blanton, C., McHugh, C., Nikonov, S., Radhakrishnan, A., ... Zhang, R. (2018a). *Noaa-gfdl gfdl-cm4 model output.* Earth System Grid Federation. Retrieved from `https://doi.org/10.22033/ESGF/CMIP6.1402` doi: 10.22033/ESGF/CMIP6.1402

Guo, H., John, J. G., Blanton, C., McHugh, C., Nikonov, S., Radhakrishnan, A., ... Zhang, R. (2018b). *Noaa-gfdl gfdl-cm4 model output prepared for cmip6 scenariomip.* Earth System Grid Federation. Retrieved from `https://doi.org/10.22033/ESGF/CMIP6.9242` doi: 10.22033/ESGF/CMIP6.9242

Hajima, T., Abe, M., Arakawa, O., Suzuki, T., Komuro, Y., Ogura, T., ... Tachiiri, K. (2019). *Miroc miroc-es2l model output prepared for cmip6 cmip.* Earth System Grid Federation. Retrieved from `https://doi.org/10.22033/ESGF/CMIP6.902` doi: 10.22033/ESGF/CMIP6.902

Harper, S. (2000). Thermocline ventilation and pathways of tropical–subtropical water mass exchange. *Tellus A: Dynamic Meteorology and Oceanography*, *52*(3), 330–345.

Henson, S. A., Sanders, R., & Madsen, E. (2012). Global patterns in efficiency of particulate organic carbon export and transfer to the deep ocean. *Global Biogeochemical Cycles*, *26*(1), n/a–n/a.

Heuzé, C. (2020). Antarctic bottom water and north atlantic deep water in cmip6 models.

Ito, T., Minobe, S., Long, M. C., & Deutsch, C. (2017). Upper ocean o2 trends: 1958-2015. *Geophysical Research Letters*, *44*(9), 4214–4223.

John, J. G., Blanton, C., McHugh, C., Radhakrishnan, A., Rand, K., Vahlenkamp, H., ... Zeng, Y. (2018). *Noaa-gfdl gfdl-esm4 model output prepared for cmip6 scenariomip.* Earth System Grid Federation. Retrieved from `https://doi.org/10.22033/ESGF/CMIP6.1414` doi: 10.22033/ESGF/CMIP6.1414

Jungclaus, J., Bittner, M., Wieners, K.-H., Wachsmann, F., Schupfner, M., Legutke, S., ... Roeckner, E. (2019). *Mpi-m mpiesm1.2-hr model output prepared for cmip6 cmip.* Earth System Grid Federation. Retrieved from `https://doi.org/10.22033/ESGF/CMIP6.741` doi: 10.22033/ESGF/CMIP6.741

Karnauskas, K. B., Jakoboski, J., Johnston, T. M. S., Owens, W. B., Rudnick, D. L., & Todd, R. E. (2020). The pacific equatorial undercurrent in three generations of global climate models and glider observations. *Journal of Geophysical*

Research: Oceans, *125*(11).

Keeling, R. F., Körtzinger, A., & Gruber, N. (2010). Ocean deoxygenation in a warming world. *Annual Review of Marine Science*, *2*(1), 199–229.

Koeve, W., & Kähler, P. (2016). Oxygen utilization rate (our) underestimates ocean respiration: A model study. *Global Biogeochemical Cycles*, *30*(8), 1166–1182.

Krasting, J. P., John, J. G., Blanton, C., McHugh, C., Nikonov, S., Radhakrishnan, A., ... Zhao, M. (2018). *Noaa-gfdl gfdl-esm4 model output prepared for cmip6 cmip.* Earth System Grid Federation. Retrieved from `https://doi.org/10.22033/ESGF/CMIP6.1407` doi: 10.22033/ESGF/CMIP6.1407

Kwiatkowski, L., Bopp, L., Aumont, O., Ciais, P., Cox, P. M., Laufkötter, C., ... Séférian, R. (2017). Emergent constraints on projections of declining primary production in the tropical oceans. *Nature Climate Change*, *7*(5), 355–358.

Kwiatkowski, L., Torres, O., Bopp, L., Aumont, O., Chamberlain, M., Christian, J., ... Ziehn, T. (2020). Twenty-first century ocean warming, acidification, deoxygenation, and upper ocean nutrient decline from cmip6 model projections.

Lachkar, Z., Smith, S., Lévy, M., & Pauluis, O. (2016). Eddies reduce denitrification and compress habitats in the arabian sea. *Geophysical Research Letters*, *43*(17), 9148–9156.

Lam, P., & Kuypers, M. (2011). Microbial nitrogen cycling processes in oxygen minimum zones. *Ann Rev Mar Sci*, *3*, 317–345.

Levin, L. A. (2018). Manifestation, drivers, and emergence of open ocean deoxygenation. *Annual Review of Marine Science*, *10*(1), 229–260.

Llanillo, P. J., Pelegrí, J. L., Talley, L. D., Peña-Izquierdo, J., & Cordero, R. R. (2018). Oxygen pathways and budget for the eastern south pacific oxygen minimum zone. *Journal of Geophysical Research: Oceans*.

Locarnini, R., Mishonov, A., Antonov, J., Boyer, T., Garcia, H., Baranova, O., ... others (2013). World ocean atlas 2013, volume 1: Temperature, edited by: Levitus, s. *A. Mishonov Technical Ed., NOAA Atlas NESDIS*, *73*, 40.

Long, M. C., Deutsch, C., & Ito, T. (2016). Finding forced trends in oceanic oxygen: Trends in dissolved oxygen. *Global Biogeochemical Cycles*, *30*(2), 381–397.

Luyten, J., Pedlosky, J., & Stommel, H. (1983). The ventilated thermocline. *Journal of Physical Oceanography*, *13*(2), 292–309.

Lévy, M., Resplandy, L., Palter, J., Couespel, D., & Lachkar, Z. (2021). The crucial contribution of mixing to present and future ocean oxygen distribution. *hal.archives-ouvertes.fr*.

Palter, J. B., & Trossman, D. S. (2018). The sensitivity of future ocean oxygen to changes in ocean circulation. *Global Biogeochemical Cycles*, *32*(5), 738–751.

Paulmier, A., & Ruiz-Pino, D. (2009). Oxygen minimum zones (omzs) in the modern ocean. *Progress in Oceanography*, *80*(3), 113–128.

Pedlosky, J. (1986). The buoyancy and wind-driven ventilated thermocline. *Journal of physical oceanography*, *16*(6), 1077–1087.

Petrie, R., Denvil, S., Ames, S., Levavasseur, G., Fiore, S., Allen, C., ... Wagner, R. (2021). Coordinating an operational data distribution network for cmip6 data. *Geoscientific Model Development*, *14*(1), 629–644.

Resplandy, L. (2018). Will ocean zones with low oxygen levels expand or shrink. *Nature*, *557*(7705), 314.

Schmidtko, S., Stramma, L., & Visbeck, M. (2017). Decline in global oceanic oxygen content during the past five decades. *Nature*, *542*(7641), 335.

Schupfner, M., Wieners, K.-H., Wachsmann, F., Steger, C., Bittner, M., Jungclaus, J., ... Roeckner, E. (2019). *Dkrz mpi-esm1.2-hr model output prepared for cmip6 scenariomip.* Earth System Grid Federation. Retrieved from `https://doi.org/10.22033/ESGF/CMIP6.2450` doi: 10.22033/ESGF/CMIP6.2450

Seferian, R. (2018). *Cnrm-cerfacs cnrm-esm2-1 model output prepared for cmip6 cmip.* Earth System Grid Federation. Retrieved from `https://doi.org/10.22033/ESGF/CMIP6.1391` doi: 10.22033/ESGF/CMIP6.1391

Seferian, R. (2019). *Cnrm-cerfacs cnrm-esm2-1 model output prepared for cmip6 scenariomip.* Earth System Grid Federation. Retrieved from `https://doi.org/10.22033/ESGF/CMIP6.1395` doi: 10.22033/ESGF/CMIP6.1395

Seland, y., Bentsen, M., Oliviè, D. J. L., Toniazzo, T., Gjermundsen, A., Graff, L. S., ... Schulz, M. (2019a). *Ncc noresm2-lm model output prepared for cmip6 cmip.* Earth System Grid Federation. Retrieved from `https://doi.org/10.22033/ESGF/CMIP6.502` doi: 10.22033/ESGF/CMIP6.502

Seland, y., Bentsen, M., Oliviè, D. J. L., Toniazzo, T., Gjermundsen, A., Graff, L. S., ... Schulz, M. (2019b). *Ncc noresm2-lm model output prepared for cmip6 scenariomip.* Earth System Grid Federation. Retrieved from `https://doi.org/10.22033/ESGF/CMIP6.604` doi: 10.22033/ESGF/CMIP6.604

Shigemitsu, M., Yamamoto, A., Oka, A., & Yamanaka, Y. (2017). One possible uncertainty in cmip5 projections of low oxygen water volume in the eastern tropical pacific. *Global Biogeochemical Cycles*, *31*(5), 804–820.

Siegel, D. A., Buesseler, K. O., Doney, S. C., Sailley, S. F., Behrenfeld, M. J., & Boyd, P. W. (2014). Global assessment of ocean carbon export by combining satellite observations and food-web models. *Global Biogeochemical Cycles*, *28*(3), 181–196.

Stock, C. A., Dunne, J. P., Fan, S., Ginoux, P., John, J., Krasting, J. P., ... Zadeh, N. (2020). Ocean biogeochemistry in gfdl's earth system model 4.1 and its response to increasing atmospheric co 2. *Journal of Advances in Modeling Earth Systems*, *12*(10).

Stramma, L., Johnson, G. C., Firing, E., & Schmidtko, S. (2010). Eastern pacific oxygen minimum zones: Supply paths and multidecadal changes. *Journal of Geophysical Research: Oceans*, *115*(C9).

Stramma, L., Johnson, G. C., Sprintall, J., & Mohrholz, V. (2008). Expanding oxygen-minimum zones in the tropical oceans. *Science*, *320*(5876), 655–658.

Stramma, L., Prince, E. D., Schmidtko, S., Luo, J., Hoolihan, J. P., Visbeck, M., ... Körtzinger, A. (2012). Expansion of oxygen minimum zones may reduce available habitat for tropical pelagic fishes. *Nature Climate Change*, *2*(1), 33–37.

Swart, N. C., Cole, J. N., Kharin, V. V., Lazare, M., Scinocca, J. F., Gillett, N. P., ... Sigmond, M. (2019b). *Cccma canesm5-canoe model output prepared for cmip6 cmip.* Earth System Grid Federation. Retrieved from `https://doi.org/10.22033/ESGF/CMIP6.10205` doi: 10.22033/ESGF/CMIP6.10205

Swart, N. C., Cole, J. N., Kharin, V. V., Lazare, M., Scinocca, J. F., Gillett, N. P., ... Sigmond, M. (2019c). *Cccma canesm5-canoe model output prepared for cmip6 scenariomip.* Earth System Grid Federation. Retrieved from `https://doi.org/10.22033/ESGF/CMIP6.10207` doi: 10.22033/ESGF/CMIP6.10207

Swart, N. C., Cole, J. N., Kharin, V. V., Lazare, M., Scinocca, J. F., Gillett, N. P., ... Sigmond, M. (2019d). *Cccma canesm5 model output prepared for cmip6 cmip.* Earth System Grid Federation. Retrieved from `https://doi.org/10.22033/ESGF/CMIP6.1303` doi: 10.22033/ESGF/CMIP6.1303

Swart, N. C., Cole, J. N., Kharin, V. V., Lazare, M., Scinocca, J. F., Gillett, N. P., ... Sigmond, M. (2019e). *Cccma canesm5 model output prepared for cmip6 scenariomip.* Earth System Grid Federation. Retrieved from `https://doi.org/10.22033/ESGF/CMIP6.1317` doi: 10.22033/ESGF/CMIP6.1317

Swart, N. C., Cole, J. N. S., Kharin, V. V., Lazare, M., Scinocca, J. F., Gillett, N. P., ... Winter, B. (2019a). The canadian earth system model version 5 (canesm5.0.3). *Geoscientific Model Development*, *12*(11), 4823–4873.

Tachiiri, K., Abe, M., Hajima, T., Arakawa, O., Suzuki, T., Komuro, Y., ... Kawamiya, M. (2019). *Miroc miroc-es2l model output prepared for cmip6 scenariomip.* Earth System Grid Federation. Retrieved from `https://doi.org/10.22033/ESGF/CMIP6.936` doi: 10.22033/ESGF/CMIP6.936

Talley, L. D., Pickard, G. L., Emery, W. J., & Swift, J. H. (2011). Chapter 10

- pacific ocean. In L. D. Talley, G. L. Pickard, W. J. Emery, & J. H. Swift (Eds.), *Descriptive physical oceanography (sixth edition)* (Sixth Edition ed., p. 303-362). Boston: Academic Press. Retrieved from https://www.sciencedirect.com/science/article/pii/B9780750645522100101 doi: https://doi.org/10.1016/B978-0-7506-4552-2.10010-1

Tang, Y., Rumbold, S., Ellis, R., Kelley, D., Mulcahy, J., Sellar, A., ... Jones, C. (2019). *Mohc ukesm1.0-ll model output prepared for cmip6 cmip.* Earth System Grid Federation. Retrieved from https://doi.org/10.22033/ESGF/CMIP6.1569 doi: 10.22033/ESGF/CMIP6.1569

Taylor, K. E., Stouffer, R. J., & Meehl, G. A. (2011). An overview of cmip5 and the experiment design. *Bulletin of the American Meteorological Society Bull. Amer. Meteor. Soc.*, *93*(4), 485–498.

Vaquer-Sunyer, R., & Duarte, C. M. (2008). Thresholds of hypoxia for marine biodiversity. *Proceedings of the National Academy of Sciences*, *105*(40), 15452–15457.

Wieners, K.-H., Giorgetta, M., Jungclaus, J., Reick, C., Esch, M., Bittner, M., ... Roeckner, E. (2019a). *Mpi-m mpiesm1.2-lr model output prepared for cmip6 cmip.* Earth System Grid Federation. Retrieved from https://doi.org/10.22033/ESGF/CMIP6.742 doi: 10.22033/ESGF/CMIP6.742

Wieners, K.-H., Giorgetta, M., Jungclaus, J., Reick, C., Esch, M., Bittner, M., ... Roeckner, E. (2019b). *Mpi-m mpiesm1.2-lr model output prepared for cmip6 scenariomip.* Earth System Grid Federation. Retrieved from https://doi.org/10.22033/ESGF/CMIP6.793 doi: 10.22033/ESGF/CMIP6.793

Yang, S., Gruber, N., Long, M. C., & Vogt, M. (2017). Enso-driven variability of denitrification and suboxia in the eastern tropical pacific ocean. *Global Biogeochemical Cycles*, *31*(10), 1470–1487.

Yukimoto, S., Koshiro, T., Kawai, H., Oshima, N., Yoshida, K., Urakawa, S., ... Adachi, Y. (2019a). *Mri mri-esm2.0 model output prepared for cmip6 cmip.* Earth System Grid Federation. Retrieved from https://doi.org/10.22033/ESGF/CMIP6.621 doi: 10.22033/ESGF/CMIP6.621

Yukimoto, S., Koshiro, T., Kawai, H., Oshima, N., Yoshida, K., Urakawa, S., ... Adachi, Y. (2019b). *Mri mri-esm2.0 model output prepared for cmip6 scenariomip.* Earth System Grid Federation. Retrieved from https://doi.org/10.22033/ESGF/CMIP6.638 doi: 10.22033/ESGF/CMIP6.638

Zhuang, J., raphael dussin, Huard, D., Bourgault, P., Banihirwe, A., Hamman, J., ... et al. (2021, February). *pangeo-data/xesmf: v0.5.2.* Zenodo. Retrieved from https://doi.org/10.5281/zenodo.4464833 doi: 10.5281/zenodo.4464833

Ziehn, T., Chamberlain, M., Lenton, A., Law, R., Bodman, R., Dix, M., ... Druken, K. (2019a). *Csiro access-esm1.5 model output prepared for cmip6 cmip.* Earth System Grid Federation. Retrieved from https://doi.org/10.22033/ESGF/CMIP6.2288 doi: 10.22033/ESGF/CMIP6.2288

Ziehn, T., Chamberlain, M., Lenton, A., Law, R., Bodman, R., Dix, M., ... Druken, K. (2019b). *Csiro access-esm1.5 model output prepared for cmip6 scenariomip.* Earth System Grid Federation. Retrieved from https://doi.org/10.22033/ESGF/CMIP6.2291 doi: 10.22033/ESGF/CMIP6.2291

Zweng, J. R. J. A. R. L. A. M. T. B. H. G. O. B. D. J. D. M. B., M.M. (2013). World ocean atlas 2013, volume 2: Salinity, edited by: Levitus, s. *A. Mishonov Technical Ed., NOAA Atlas NESDIS*, *74*.